SUPPLEMENTAL FIGURES

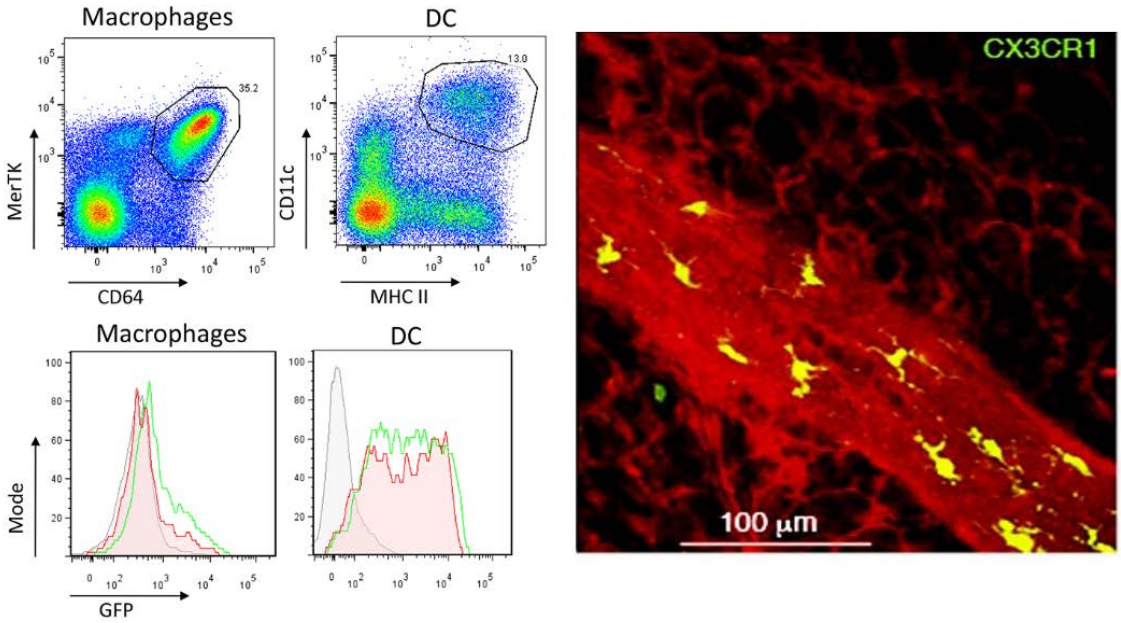

Supplementary Figure 1. CX3CR1^{+} cells in perinodal adipose tissue are DCs. To determine if CX3CR1^{+} cells in perinodal fat around the brachial lymph node were macrophages, DCs, or otherwise, we gated on macrophages as MerTK^{+} CD64^{+} cells and then identified CD11c^{+} MHC II^{+} cells within the MerTK^{-} CD64^{-} gate as DCs. CX3CR1$^{gfp/+}$ expression was mainly confined to DCs, although macrophages showed some autofluorescence in the same channel, as typical for macrophages. We visualized the major collecting lymphatic vessel in the fat by allowing it to transport red fluorescent dextran injected into scapular skin that drains to this fat pad and lymph node. CX3CR1$^{gfp/+}$ cells, evidently DCs based on flow cytometry, were closely associated with the transport lymphatic vessel.

SUPPLEMENTAL FIGURES

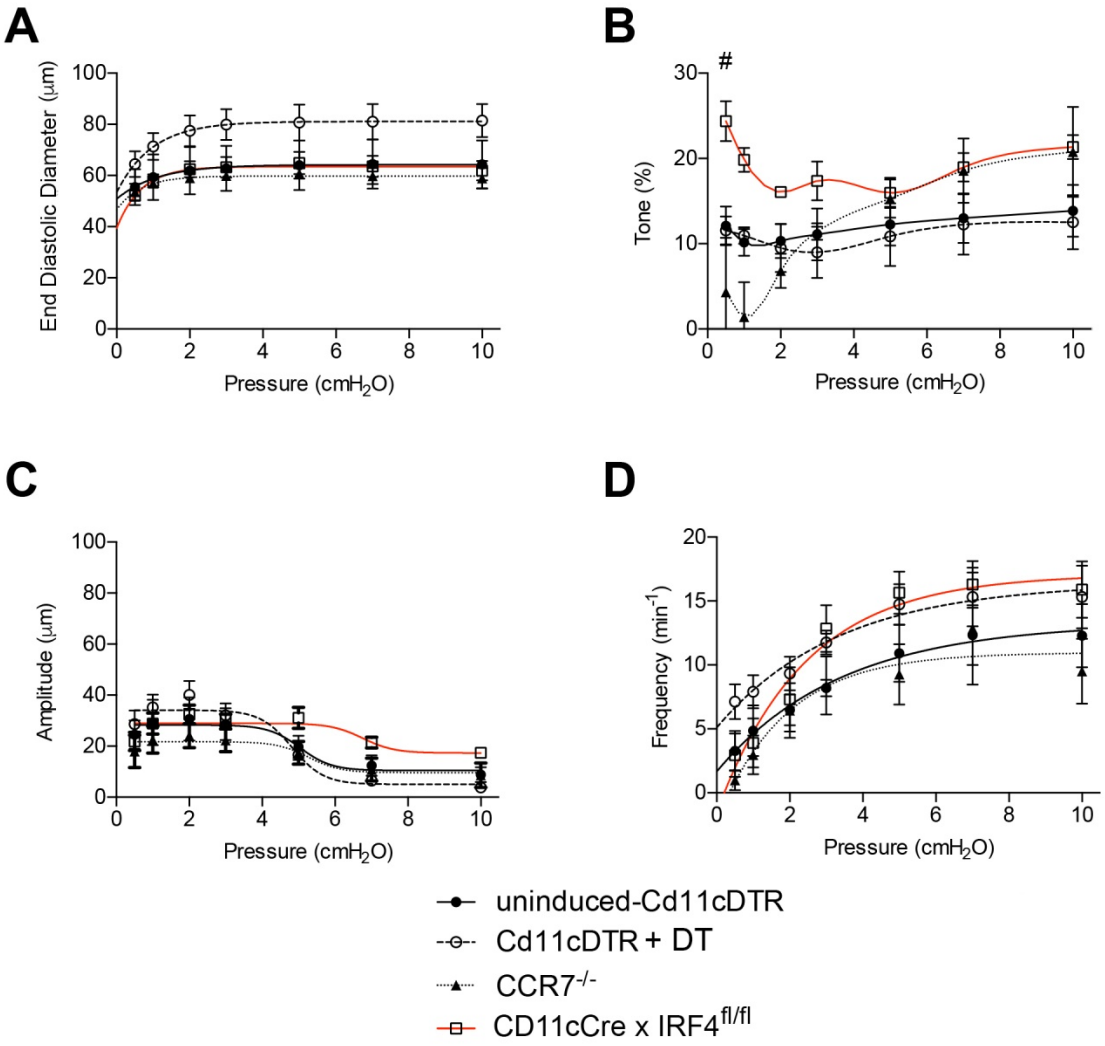

Supplemental Figure 2. Functional properties of exteriorized lymphatic collecting vessels subjected to stepwise increases in pressure are unchanged in response to CCR7 deficiency or loss of IRF4 in DCs. Cannulated popliteal afferent collecting vessels were prepared and subjected to a pressure gradient as described previously (1). End diastolic diameter and the tone, amplitude, and frequency of lymphatic contractions were recorded. Control mice were CD11c-DTR transgenic mice not treated with DT (C57BL/6 background). N= 3-4 for each genotype. None of the patterns of responses were statistically significant, as analyzed using 2-way ANOVA.

SUPPLEMENTAL FIGURES

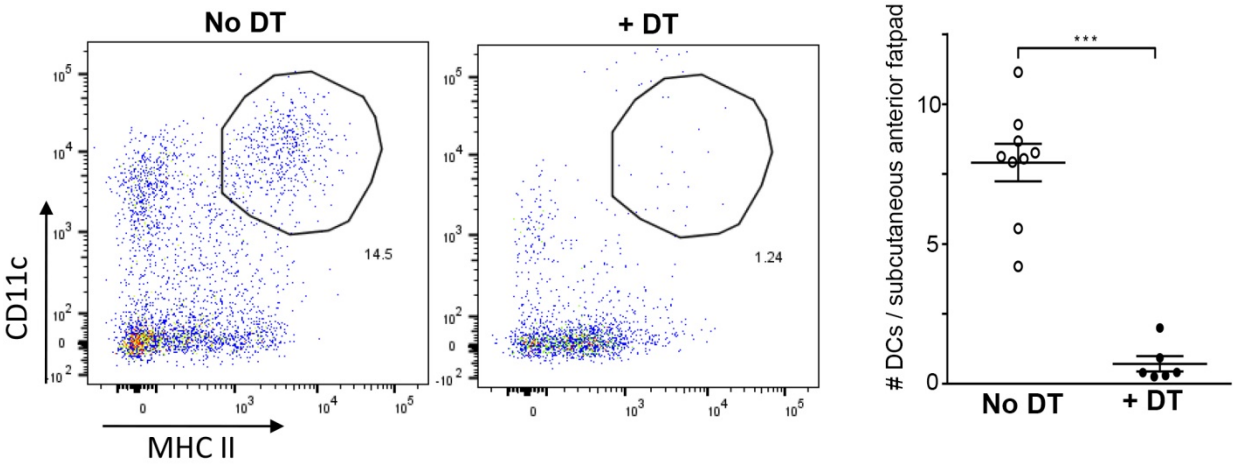

Supplementary Figure 3. Diptheria toxin-mediated depletion of dendritic cells in the adipose tissue surrounding the brachial lymph node (anterior subcutaneous fat). Diptheria toxin was withheld from (no DT) or given to (+DT) CD11c-DTR mice. 36 hours after DT administration, single cell suspensions of the vascular-stromal fraction of fat pads (2 per mouse, left and right) from individual mice were analyzed for DCs ($CD11c^+$ and $MHC\ II^+$) after pregating on $CD45^+$ singlet events. Graph on the right shows data from individual mice normalized to the number of DCs in one fat pad. Six to nine mice per group were analyzed. For statistical evaluation, data were assessed using Mann-Whitney test, *p<0.05, **p<0.01, ***p<0.001 and ****p<0.0001.

SUPPLEMENTAL FIGURES

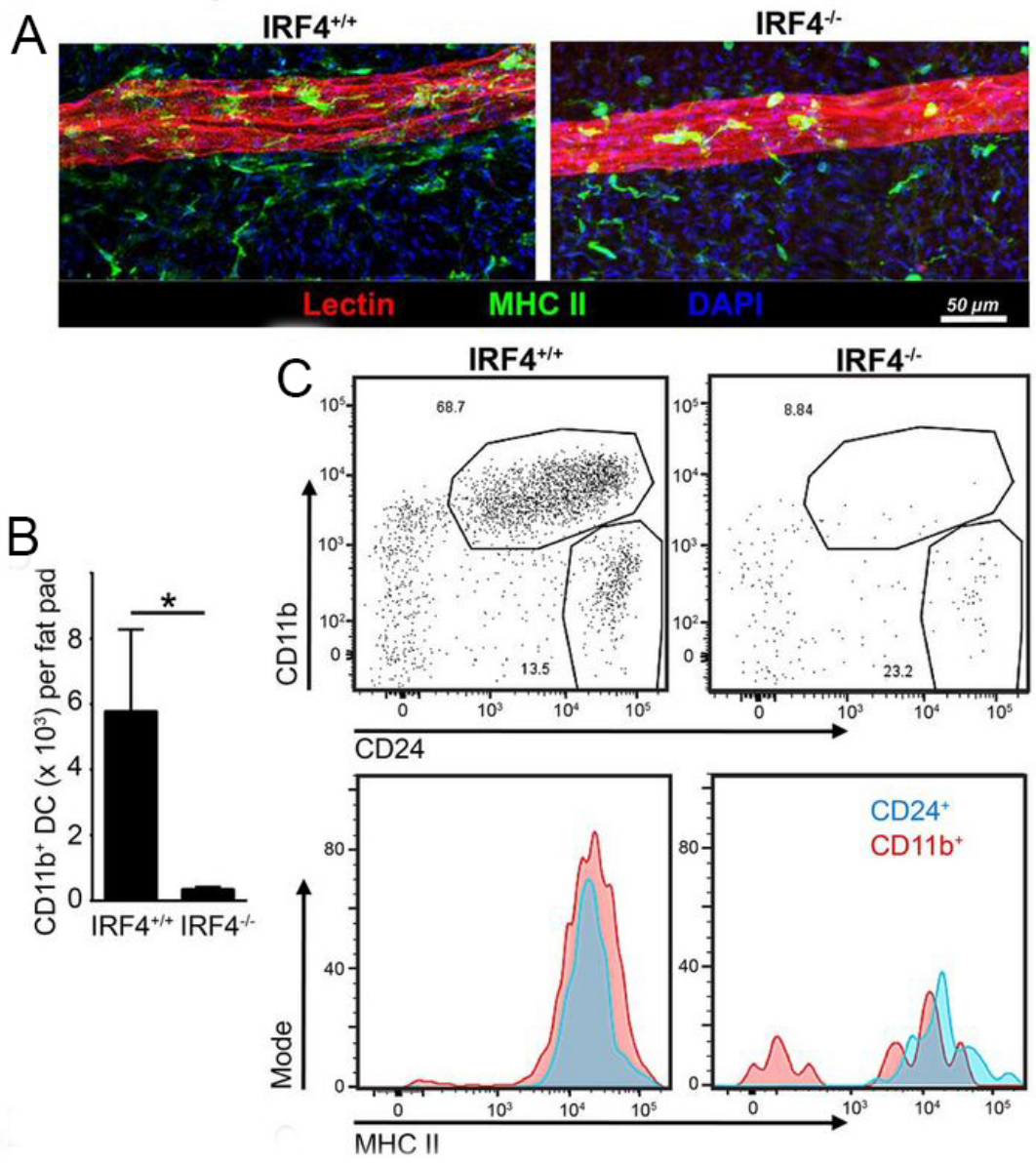

Supplementary Figure 4. Analysis of DC subsets in IRF4$^{-/-}$ mice. (A) Confocal microscopy analysis of the perinodal adipose tissue of IRF4$^{+/+}$ and IRF4$^{-/-}$ mice. The lymphatic collector was labelled via s.c. injection of DyLight 594-conjugated lectin (Red) and cells were stained for MHC II (green) and nuclear staining for DAPI (blue). (B, C) Flow cytometric analysis of the CD11b^{+} DC in the perinodal adipose tissue of IRF4$^{+/+}$ and IRF4$^{-/-}$ mice. Four to five mice per genotype were analyzed. For statistical evaluation, data were assessed using Mann-Whitney test, *p<0.05.

SUPPLEMENTAL FIGURES

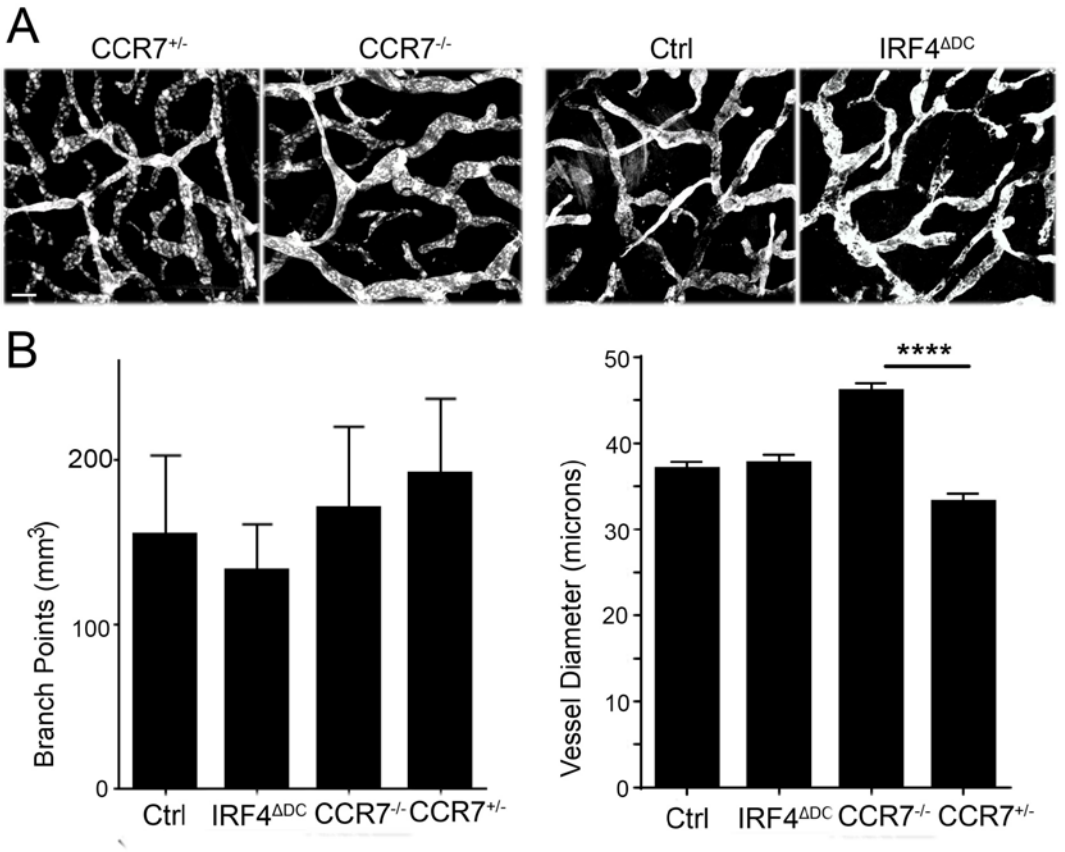

Supplementary Figure 5. Evaluation of lymphatic capillaries in the absence of CCR7 or IRF4-dependent DCs. A) Photomicrographs that typify the pattern of lymphatic capillaries observed in mouse ear in different genotypes. In $CCR7^{+/-}$ and $CCR7^{-/-}$ genotypes, capillaries were visualized using Prox1-driven Tomato reporter crossed to these genotypes. For studies using $IRF4^{\Delta DC}$ and controls (Ctrl; $IRF4^{fl/fl}$ mice), lymphatic capillaries were visualized by staining for LYVE-1. Size bar applies to all images, 100 μm. B) The density of branch points and width of vessels in the lymphatic capillary networks were evaluated using 2-5 images per mouse with n=3 mice examined per genotype. Statistics were carried out using one-way ANOVA, followed by Tukey's post hoc test, with one relationship showing statistical significance, $p < 0.001$.

SUPPLMENTAL FIGURE REFERENCES

1. Scallan JP and Davis MJ: Genetic removal of basal nitric oxide enhances contractile activity in isolated murine collecting lymphatic vessels. **J Physiology** 591(8):2139-2156, 2013.

MOVIE LEGENDS

Movie 1:

Two representative movies from CD11c-YFP CCR7$^{+/+}$ (left) and CD11c-YFP CCR7$^{-/-}$ mice (right). QDOT^{Tm} were s.c. administered in the footpad to label the lymphatic vasculature. Green, YFP+ DCs; red, QDOT tracer; blue, 2nd harmonic signal indicative of collagen. Note one YFP+ cell on the left extending a pseudopod through blue lymphatic vessel wall toward the lumen that is highlighted by QDOT tracer. At one point in the movie, there is a rapid flash of a YFP+ cell in the lymphatic lumen, likely from a DC passing through the vessel toward the popliteal lymph node after entering lymphatic capillaries in the skin.

Movie 2:

Prox1-cre-TdTomato-CD11c-YFP-CCR7$^{+/-}$ mice were fed a tamoxifen-enriched diet (Harlan) for 3 weeks. Mice were analyzed by 2-photon intravital microscopy as described in the Methods section. Representative video is shown with particular focus on the lymphatic collector vessel. A z-projection is first shown, followed by a 3-dimensional rotation of the vessel including a view of its full cross-section, followed by live imaging. Green, YFP+ DCs; red, Tomato protein expressed by lymphatic endothelium; blue, 2nd harmonic signal indicative of collagen. Scale bar 50 μm.

Movie 3:

Prox1-cre-TdTomato-CD11c-YFP-CCR7$^{+/-}$ mice were fed a tamoxifen-enriched diet (Harlan) for 3 weeks. Mice were analyzed by 2-photon intravital microscopy as described in the Methods section. Representative video is shown with particular focus on the lymphatic collecting vessel valve. The valve is observed near the lower part of the vessel in the video with two valve leaflets forming a tulip-like shape upward in the lumen of the vessel. A z-projection is first shown, followed by a 3-dimensional rotation of the vessel including a view its full cross-section and with the valve rotating toward the top of the video, followed by live imaging. Green, YFP+ DCs; red, Tomato protein expressed by lymphatic endothelium; blue, 2nd harmonic signal indicative of collagen. Scale bar 50 μm.

Movie 4:

Method for estimating the surface area of the lymphatic vessel in contact with dendritic cells. Vessel and cells were modeled in Imaris and then exported into MATLAB, where contact of vessel and cell was determined. The contact was then reduced in dimensionality from 3D to 2D via singular value decomposition. The boundary of the 2D point cloud was found by creating its convex hull, and then the area within boundary was calculated.